Supporting Information

REVISED

RECEIVED
APR 2 9 2002
IN FINAL FORM
JOURNAL OF PHYSICAL CHEMISTRY

for the article

Computational Study of the Mechanism and Product Yields in the Reaction Systems $C_2H_3 + CH_3 \rightleftarrows C_3H_6 \rightleftarrows H + C_3H_5$ and $C_2H_3 + CH_3 \rightarrow CH_4 + C_2H_2$.

Stanislav I. Stoliarov,[a, †] Vadim D. Knyazev,[*, a, b] Irene R. Slagle [a]

[a)] Research Center for Chemical Kinetics

Department of Chemistry

The Catholic University of America

Washington, DC 20064

[b)] National Institute of Standards and Technology

Physical and Chemical Properties Division

Gaithersburg, MD 20899

[*] Corresponding author. E-mail: knyazev@cua.edu.

[†] Current address: Department of Chemical Engineering, University of Massachusetts, Amherst, MA 01003

IS. Analysis of the Potential Energy Surface of Reaction 1. Reaction Mechanism and Product Channels.

IS.1. Computational Methods.

Two main computational approaches were employed in this study. The first approach is the widely used Gaussian 2 (G2) method.[1] In this method, final geometry optimization is performed at the MP2/6-31G(d) level (although the lower HF/6-31G(d) level is used for vibrational mode analysis) and then single-point energy is obtained from a series of MP and QCISD(T) calculations[2] approximating a QCISD(T)/6-311+G(3df,2p) value. In the second computational approach, the B3PW91 density functional method[3,4] was used for geometry optimization. The choice of the B3PW91 functional was based on the conclusions of Cui and co-authors[5] who examined the performance of a number of density functional methods and the MP2 method on a system similar to that of reaction 1 (formation of $CH_3 + C_2H_3^+$, $C_3H_4^+ + H_2$, and $C_3H_5^+ + H$ in the $CH_4 + C_2H_2^+$ reaction). These authors have found the B3PW91 method to produce the most reliable structures. This density functional method was used together with the 6-31G(d,p) Gaussian basis set. Additional polarization *p* functions on hydrogen atoms used in this basis set (as compared to the 6-31G(d) set used for geometry optimization in the G2 method) are believed to provide a better description of the H-bridged structures that represent a significant part of the potential energy surface under study. Frequency analysis and zero-point vibrational energy calculations in the second approach were performed at the same B3PW91/6-31G(d,p) level of theory. For single point energy calculations of the B3PW91 optimized structures, the QCISD(T) method with the 6-311+G(2df,2p) Gaussian basis set was employed. The QCISD(T) configuration interaction method was extensively tested on various species and shown to be very efficient in capturing most of the electron correlation energy necessary for accurate treatment of energetics.[6]

The two approaches (G2 and QCISD(T)//B3PW91) were chosen to provide similar high accuracy together with reasonable computational speed. Both of them were used for each structure on the potential energy surface under study in order to assess the reliability of the results. Restricted methods were used for closed-shell structures and unrestricted methods were used for radicals. The stability of self-consistent-field (SCF) solutions was tested for each optimized geometry. In cases where restricted methods generated unstable wavefunctions, unrestricted methods were employed to obtain stable SCF solutions (with the exception of G2

energies, in which case closed-shell calculations were performed for all non-radical species). All stationary points were positively identified as minimum (no imaginary frequencies) or saddle point (one imaginary frequency). Intrinsic reaction coordinate (IRC)[7] calculations in mass-weighted internal coordinates[8] were performed for each optimized saddle point structure in order to verify the connected reactants and products. All calculations were carried out using the Gaussian 98[9] and Gaussian 94[10] packages of programs.

IS.2. Decomposition and Isomerization of Chemically Activated Propene.

Several saddle points corresponding to transformations of propene were found using the computational methods described above. Structures of these saddle points and some important intermediates are presented in Table 1S, where structures of all stable species involved in reaction channels 1a – 1g obtained in the calculations are given. Calculated energies of all individual species are listed in Table 3S (absolute energies) and Table 2 of the article (energies of transition states and products relative to the C_2H_3 + CH_3 reactants). A potential energy diagram of reaction 1 obtained from the experimental thermochemical data and from the results of the calculations is presented in Figure 1 of the article. Individual channels of propene transformation are discussed below.

Isomerization to cyclopropane (channel 1d)

The optimized structure of the transition state of this reaction, TS1, is given in Table 1S. B3PW91-level IRC analysis shows that TS1 leads directly from propene to cyclopropane. IRC calculations performed at the MP2 level of theory indicate that TS1 leads from propene to a shallow minimum, a trimethylene intermediate. A low-energy transition state located at the MP2 level leads from this minimum to cyclopropane, according to the IRC analysis. However, G2 calculations performed using the MP2-optimized structures demonstrate a monotonic energy decrease along the TS1→cyclopropane path, thus indicating the absence of both the trimethylene intermediate and the trimethylene-cyclopropane transition state. The results of a recent computational study of isomerization of cyclopropane to propene[11] performed at the B3LYP/cc-pVDZ level of theory also indicate that there is no intermediate on the reaction path and that the reaction occurs via a saddle point almost identical in structure to TS 1 that leads directly from the reactant to the product. High spin contamination of the HF wave function of the TS1 structure

($<s^2>$=0.86, see Table 3S.) may indicate that it is a singlet biradical (two unpaired electrons with opposite spin). However, the analysis of the molecular orbital occupation for this transition state performed by the authors of reference 11 at the TCSCF/cc-pVDZ level of theory indicates that it is a closed-shell singlet (all electrons are paired) with only some biradical character.

The energies of the TS1 transition state calculated by the G2 and QCISD(T)//B3PW91 methods differ by 37 kJ mol^{-1}. This disagreement between the results of the two approaches is most likely due to the high spin contamination of the TS 1 structure. Furue and Pacey[12] examined a large volume of experimental kinetic data available on the reaction of the isomerization of cyclopropane to propene. These authors recommended the high-pressure-limit activation energy value of 276.0 ± 2 kJ mol^{-1} for this reaction. Thus, the value of the barrier height for the isomerization of propene to cyclopropane can be estimated using the experimental thermochemical data (Table 1 of the article) as 309 kJ mol^{-1}. This value coincides with the average of the G2 and QCISD(T)//B3PW91 relative energies of TS1 (Table 2 of the article).

H_2 elimination (channels 1e, 1f, and 1g)

Elimination of molecular hydrogen is one of the possible routes of decomposition of chemically activated propene (product channels 1e, 1f, or 1g). A scan of the potential energy surface performed at the HF/6-31G(d) and B3PW91/6-31G(d,p) levels of theory revealed no four-center H_2 elimination transition states. No transition state could be located for the reaction of H_2 elimination that would lead to the formation of cyclopropene (product channel 1g) as well. However, four different pathways of three-center H_2 elimination were identified. The optimized geometries of the transition states and intermediates of these reactions are presented in Table 1S.

Two of these pathways (proceeding through saddle points TS2.1 and TS2.2) are similar in structure and energy. They involve H_2 elimination from the terminal vinylic carbon of the propene molecule. H_2 elimination occurs simultaneously with a shift of the hydrogen atom from the middle to the terminal carbon atom. B3PW91 and MP2-level IRC calculations performed for these transition states show that both lead directly from propene to propyne + H_2.

Two other pathways of H_2 elimination proceed via an H-atom shift transition state, TS2.3, that leads to the formation of the CH_3CCH_3 intermediate, which is a spin-contaminated singlet. Three-center H_2 elimination from the CH_3CCH_3 intermediate via either the TS2.4 or the

TS2.5 saddle points leads to the formation of propyne. No reaction pathways corresponding to H_2 elimination from the methyl group of propene could be located.

The results of the energy calculations for the species involved in the H_2 elimination reactions (Table 2 of the article) demonstrate an excellent agreement between the G2 and the QCISD(T)//B3PW91 methods. The potential energy profiles of the H_2 elimination pathways are shown in Figure 1 of the article. Although the energies of TS2.1 and TS2.2 are slightly below that of the $C_2H_3 + CH_3$ reactants, they are 26 – 43 kJ mol^{-1} above the energy of the $C_3H_5 + H$ decomposition channel. The heights of the barriers and the "tightness"[13,14] of the TS2.1 and TS2.2 transition states (See Table 2S in the Supplement for computed frequencies.) compared to the $C_3H_5 + H$ channel barrierless decomposition make these H_2 elimination product channels unimportant under any set of conditions. The other two H_2 elimination pathways proceed via the low-energy TS2.3 transition state and the CH_3CCH_3 intermediate followed by either TS2.4 or TS2.5. The energies of the transition states TS2.4 and TS2.5 are 50 and 10 kJ mol^{-1} above the energy of the reactants, respectively (at the G-2 level). Therefore, H_2 elimination reactions can not be of any importance for chemically activated propene decomposition in the $C_2H_3 + CH_3$ system. This conclusion is supported by experimental observations: no C_3H_4 products were detected in our earlier experimental study of reaction 1.[15]

Decomposition of propene to C_2H_2 and CH_4 products (potential routes to product channel 1c)

In order to verify the hypothesis that the experimentally detected[15-19] production of acetylene in the $C_2H_3 + CH_3$ reaction is due to a direct abstraction of a hydrogen atom from the vinyl radical by methyl radical, the potential energy surface was analyzed for the presence of reaction pathways that would lead from the chemically activated propene to the same C_2H_2 and CH_4 products. Three distinct reaction routes were identified for this process. The optimized geometries of the transition states and intermediates are presented in Table 1S. These reactions proceed via the abstraction of one of three nonequivalent vinylic hydrogens of the propene molecule by the departing methyl group. In the cases of the transition states TS3.1 and TS3.2, the migration of the hydrogen atom from the remote to the adjacent carbon (with respect to the leaving methyl group) occurs in a concerted mechanism. B3PW91 and MP2-level IRC calculations indicate that the TS3.1 and the TS3.2 transition states lead directly from propene to acetylene and methane.

The transition state TS3.3 of the abstraction of H-atom from the middle carbon of the propene molecule by the departing methyl group leads to the formation of a vinylidene intermediate (CH_2C) and methane. The vinylidene intermediate is a closed-shell structure ($^1A_1$ is the ground state), which rapidly isomerizes to acetylene via the low (2 – 7 kJ mol^{-1} above the energy of the CH_2C) transition state TS3.4. According to the IRC calculations performed at the B3PW91 level of theory, the TS3.3 transition state leads directly from propene to vinylidene and methane. The results of the MP2 IRC analysis, however, suggest that a CH_3CCH_3 intermediate is located on the reaction path leading from propene to TS3.3 (Figure 1 of the article).

For all the transition states and intermediates involved in the propene decomposition pathways, the relative energies computed at the G2 and the QCISD(T)/B3PW91 levels are in near perfect agreement with each other (Table 3S and Table 2 of the article). A 18 – 21 kJ mol^{-1} discrepancy between the calculated and experimental energies of the CH_2C intermediate does not necessarily indicate the failure of the computational method as it can be explained by the large uncertainty (± 16.7 kJ mol^{-1}) of the experimentally determined ΔH_f^0 of vinylidene (Table 1 of the article).

The high energies of the TS3.1, TS3.2, and TS3.3 transition states (Figure 1 of the article) indicate that the formation of acetylene and methane (product channel 1c) does not occur via the corresponding pathways of decomposition of the chemically activated propene. This supports a direct abstraction of H-atom from the vinyl radical by methyl radical as the mechanism of this product channel. However, it should be noted that the fact that no lower-energy $C_3H_6 \rightarrow C_2H_2 + CH_4$ pathway could be found in the current work cannot serve as a rigorous proof of the absence of such a pathway.

Decomposition to $C_2H_3 + CH_3$ and $H + C_3H_5$

Decomposition of propene to $C_2H_3 + CH_3$ (the reverse of the addition reaction) and to $H + C_3H_5$ (allyl) are barrierless, i.e., the reverse addition processes proceed without potential energy barriers. As can be seen from the reaction energetics (Table 2 and Figure 1 of the article), decomposition to $H + C_3H_5$ is the preferred channel, located 53 kJ mol^{-1} below the $C_2H_3 + CH_3$ channel on the energy scale. The G2-calculated relative energies (with respect to propene) for the products of these reactions are in excellent agreement with the experimental enthalpy values (See Table 2 of the article.). The QCISD(T)//B3PW91 method underestimates the $C_2H_3 + CH_3$ and $H + C_3H_5$ energies by ≈ 11 kJ mol^{-1}.

Detailed studies of the potential energy surfaces of both of these decomposition routes were performed in order to obtain information necessary for the RRKM / master equation modeling. This information includes the potential energy profiles and evolution of molecular structures and vibrational frequencies along the reaction paths. A detailed description of the results is presented in section III of the article and section IIS of this Supporting Information.

Formation of other, not resonantly stabilized structural isomers of the C_3H_5 radical (CH_3CCH_2 and CH_3CHCH) in the H-atom elimination from chemically activated propene is highly improbable. As demonstrated by Wang,[20] calculations performed at the G2//B3LYP/6-31G(d) level of theory indicate that the energies of the CH_3CCH_2 + H and CH_3CHCH + H products lie 29 and 46 kJ mol^{-1} above the energy of the C_2H_3 + CH_3 reactants, respectively (82 and 99 kJ mol^{-1} above the energy of the H + allyl products).

IS.3. Abstraction of Hydrogen Atom from Vinyl Radical by CH_3 (Reaction Channel 1c)

There are three distinct pathways of direct abstraction of H-atom from C_2H_3 by CH_3 corresponding to the three nonequivalent hydrogen atoms of the vinyl radical. The optimized geometries of the transition states and intermediates of these channels are presented in Table 1S. These three reaction pathways (designated as channels in this subsection) show similar behavior characterized, however, by some channel-specific features. The pathway of abstraction of the *trans* H atom (*trans* relative to H) from the $=CH_2$ group of the vinyl radical is described first and then the features specific to the other two channels are characterized.

The potential energy profiles (zero-point vibrational energy not included) of the MP2- and B3PW91-level IRC reaction paths of the first channel are shown in Figure 1S. The results of IRC[7] following in mass-weighted internal coordinates[8] indicate that this channel of the $C_2H_3+CH_3 \rightarrow C_2H_2+CH_4$ reaction proceeds via formation of a loosely bonded intermediate complex, INT4.1 (minima on the potential energy profiles), followed by the TS 4.1 transition state (maxima on the potential energy profiles) which leads to the C_2H_2 and CH_4 products. The formation of the intermediate complex from the C_2H_3 + CH_3 reactants occurs without a barrier, a fact confirmed by relaxed scans of the distance between the carbon atom of the methyl radical and the corresponding hydrogen atom of the vinyl radical performed at the MP2 and B3PW91 levels of theory.

IRC calculations were performed using the structure of the TS4.1 saddle point as the starting geometry. In the calculations performed at the B3PW91 level, IRC following did not converge completely to the minimum of the intermediate complex INT4.1. The structure of the intermediate was obtained, in this case, by further optimization of the geometry of the last successful point on the IRC path. Thus, only an approximate position along the reaction coordinate is provided for this loosely bonded complex on the B3PW91 potential energy profile (Figure 1S). Similar problems due to incomplete geometry convergence in the vicinity of the energy profile minima were encountered in the cases of IRC analysis of TS4.2 and TS4.3.

The potential energy surfaces of the abstraction channels in reaction 1 are very shallow and affected by spin contamination, thus presenting a challenge for quantum chemical computations. The MP2 method is especially vulnerable to spin contamination.[6] In order to obtain more reliable information on the barrier height on the MP2-level optimized potential energy surface, an approach similar to Petersson's IRCMax method[21] was employed. QCISD(T) single point energy calculations with the 6-311G(d,p) medium-size Gaussian basis set were performed on the structures along the MP2/6-31G(d) IRC reaction path. The results of these calculations for the first abstraction channel are shown in Figure 1S (zero-point vibrational energy is not included). A G2 energy calculation was carried out for the structure at the top of the QCISD(T)//MP2 IRC barrier, which is shifted noticeably toward the C_2H_3 + CH_3 reactants with respect to the position of the MP2-level transition state. This approach is expected to provide a more accurate upper limit of the reaction barrier height.[21] The energies of the TS4.1 transition state calculated by the G2//QCISD(T)//MP2 and the QCISD(T)//B3PW91 methods as well as G2//MP2/6-31G(d) and QCISD(T)//B3PW91 energies of the intermediate complex INT4.1 are listed in Table 4S. The G2-level results indicate that the energy of the TS4.1 transition state is 16 kJ mol^{-1} below the energy of the reactants whereas QCISD(T)//B3PW91 calculations suggest that the transition state is 18 kJ mol^{-1} above the energy of C_2H_3 + CH_3. INT4.1 is located in a deep potential energy well (42 kJ mol^{-1} below the energy of the reactants) according to the G2 results but is essentially absent (no potential energy well) according to the QCISD(T)//B3PW91 calculations.

The potential energy profiles of the MP2-level IRC reaction path of the second channel (shallow-well intermediate INT4.2, saddle point TS4.2) and the third channel (intermediate INT4.3, saddle point TS4.3) of the hydrogen abstraction reaction are presented in Figures 2S and

3S, respectively. The second channel is that of the abstraction of the *cis* hydrogen atom (*cis* relative to H) from the $=CH_2$ group of the vinyl radical, while the third channel corresponds to the abstraction of an H atom from the –CH group. These potential energy profiles are similar in shape to that obtained for the first channel (Figure 1S). A minor discontinuity of the MP2 energy profile of the third channel is, probably, caused by the imperfections of the IRC reaction path, which could be due to the closeness of the $C_2H_3 + CH_3$ combination minimum energy path on the shallow potential energy surface.

At the B3PW91 level of calculations the transition states TS4.2 and TS4.3 could not be located. The results of a relaxed scan of the distance between the H-atom of the vinyl radical and the C-atom of the methyl radical (variable *r* in Figures 2S and 3S) performed at the B3PW91/6-31G(d,p) level indicate a barrierless reaction pathway for both the second and the third channels (Figures 2S and 3S). Both the MP2-level IRC calculations and the B3PW91-level scans demonstrate that the second channel leads directly to the formation of acetylene and methane whereas the third channel proceeds through the formation of methane and a vinylidene (CH_2C) intermediate, which then isomerizes to acetylene (See potential energy diagram in Figure 1 of the article.).

The G2//QCISD(T)//MP2 calculations (selection of the transition state location along the MP2-level optimized reaction path on the basis of the single-point QCISD(T)/6-31G(d,p) energies with the subsequent G2-level energy calculation of the transition state energy) similar to those reported for the first abstraction pathway were performed for the second and the third pathways as well. The QCISD(T)/6-311+G(2df,2p)-level single point calculations were performed for the same structures as the G2 calculations because optimization of geometry at the B3PW91/6-31G(d,p) level did not produce any saddle points or bound intermediates. The G2//QCISD(T)//MP2 and QCISD(T)/6-311+G(2df,2p) energies of TS4.2 and TS4.3 together with the G2 and QCISD(T)/6-311+G(2df,2p) energies of INT4.2 and INT4.3 are given in Table 4S. The G2-level calculations predict lower energies compared to the QCISD(T)/6-311+G(2df,2p) values. However, the qualitative picture is the same at both levels of calculations for the second and the third abstraction channels: formation of a shallow-well intermediate followed by a barrier (below or slightly above the energy of the reactants). Accounting for the zero-point vibrational energy contributions does not produce significant changes to the potential energy profiles (Table 4S).

Although the quantitative results of the current study of the potential energy surface of the three H-atom abstraction channels are inconclusive, they do qualitatively identify two possible patterns for the reaction pathways. The reaction may proceed through a shallow-well, loosely bound intermediate complex followed by a transition state, the energy of which is below or slightly above the energy of the reactants. Alternatively, the reaction can be a simple barrierless process that does not involve any intermediates or saddle points. Both patterns can explain the experimentally observed negative temperature dependence of the rate constant of formation of C_2H_2 and CH_4.[15]

IIS. Model of the Chemically Activated Route of the $C_2H_3 + CH_3$ Reaction

II.1. Formulation of the Master Equation.

The temporal evolution of the system can be represented by the following two differential equations (denoted as "master equation")

$$\frac{\partial\, g_p(E,t)}{\partial\, t} = \omega \int_0^\infty \left[P_p(E,E')g_p(E',t) - P_p(E',E)g_p(E,t)\right] dE' -$$

$$-\left[k_{-A}(E)+k_D(E)+k_I(E)\right] g_p(E,t)+k_{-I}(E)g_c(E,t)+[C_2H_3][CH_3]\, K_{eq}k_{-A}(E)f_p(E) \qquad \text{(Ia)}$$

$$\frac{\partial\, g_c(E,t)}{\partial\, t} = \omega \int_0^\infty \left[P_c(E,E')g_c(E',t) - R_c(E',E)g_c(E,t)\right] dE' -$$

$$-k_{-I}(E)g_c(E,t)+k_I(E)g_p(E,t) \qquad \text{(Ib)}$$

where $g_p(E,t)$ and $g_c(E,t)$ are the energy- and time-dependent populations of propene and cyclopropane, respectively; $P_p(E,E')$ and $P_c(E,E')$ are the rate coefficients of collisional energy transfer from energy E' to energy E for the corresponding species; $k_{-A}(E)$, $k_D(E)$, $k_I(E)$, and $k_{-I}(E)$ are the microcanonical (energy-specific) rate constants of the corresponding channels in scheme II; $f_p(E)$ is the normalized Boltzmann energy distribution in the active[13,14] degrees of freedom of the propene molecule; and ω is the collision frequency with the bath gas. Here, $K_{eq} = k_A^\infty / k_{-A}^\infty$, where k_A^∞ and k_{-A}^∞ are the high-pressure-limit rate constants of the corresponding channels. The first term (under the integral sign) in equation Ia describes the collisional energy transfer, the second term describes the disappearance of propene molecules due to reactions, the third term is

due to the isomerization of cyclopropane to propene, and the last term $([C_2H_3][CH_3]K_{eq}k_{-A}(E)f_p(E))$[13,14,33] accounts for the flux of the activated propene molecules formed in the $C_2H_3 + CH_3$ recombination. The zero of the energy scale is chosen to be at the bottom of the potential energy well of propene (at the zero-point vibrational energy level) for the master equation and all the related formulations.

IIS.2. Analysis of the Reaction Paths of Propene Decomposition

Computational Method

Out of the two methods (MP2/6-31G(d) and B3PW91/6-31G(d,p)) used in the study of structures on the potential energy surface of the $C_2H_3 + CH_3$ reaction (section II of the article and section IS of this Supporting Information), the B3PW91/6-31G(d,p) density functional method was selected for use in geometry optimization and calculation of frequencies along the reaction paths of decomposition of propene. The potential energy surface of decomposition of propene to vinyl and methyl radicals (reaction –A in scheme II of the article) and to H atom and allyl radical (reaction D in scheme II of the article) is highly spin-contaminated. The choice of the computational method was based on the higher reliability of the structures and frequencies produced by density functional methods on spin-contaminated potential energy surfaces.[6]

Intrinsic reaction coordinate[7] (IRC) calculations in mass-weighted internal coordinates[8] were performed at the B3PW91/6-31G(d,p) level of theory in order to obtain structures located along the reaction paths. The IRC calculations were carried out in the "downhill" mode starting from the structure obtained by optimization of the geometry of the decomposing molecule (propene) with a fixed, large separation of the departing fragments. The initial distance between the fragments (length of the breaking C-C bond in the case of propene decomposition to methyl and vinyl radicals, length of the breaking C-H bond in the case of H-atom elimination from propene) was chosen in such a way that the calculated energy of the structure was less than 2 kJ mol^{-1} below the energy of the decomposition products. The frequencies of the structures located on the IRC reaction paths were calculated by projecting (onto the coordinate space tangent to the path) and diagonalizing the mass-weighted Hessian.[22,23] QCISD(T) single point energy calculations with the 6-311G(d,p) medium-size Gaussian basis set were performed for the B3PW91-level IRC structures in order to refine the potential energy profiles along the reaction paths. All calculations were carried out using the Gaussian 98 package of programs.[9]

Potential Energy Profiles

The calculated potential energy profiles of the reaction path of the decomposition of propene to vinyl and methyl radicals are shown in Figure 4S. The upper plot presents the results of the B3PW91-level IRC calculations together with the QCISD(T) single point energies computed for the part of the B3PW91 IRC reaction path where the variationally selected transition states are likely to be located. All energy values are given relative to propene. Zero-point vibrational energies (ZPE) of the transition structures and propene are not included in the presented energy values (ZPE were included later in the calculations of the microcanonical rate constants.). The length of the breaking C-C bond of propene was chosen as a reaction coordinate. The only function of the reaction coordinate is to provide a reference to the structures on the IRC reaction path and, therefore, the choice can be arbitrary.

The results of the B3PW91 and QCISD(T) energy calculations are in good agreement with each other (Figure 4S, upper plot). In order for the potential energy profile to conform to the experimental reaction thermochemistry, the QCISD(T) energies were scaled with the ratio of the relative experimental energy of the products (with respect to propene, ZPE not included) to that obtained in the QCISD(T) calculations. The calculated and experimental energies are listed in Table 5S. The scaled QCISD(T) energy profile is shown in the lower plot of Figure 4S.

The scaled QCISD(T) energies were interpolated with a polynomial function of the form

$$E(R) = E_{\infty}[1 - \sum_{i=1}^{8} a_i / R^i] \qquad \text{(II)}$$

where E_{∞} is the relative experimental energy of the products, R is the reaction coordinate and a_i are the fitting coefficients. The result of the interpolation is presented as a solid line in Figure 4S (the lower plot). The optimized coefficients of the polynomial expression II are given in Table 5S.

The reaction path of the decomposition of propene to allyl radical and hydrogen atom (reaction D in scheme II of the article) was analyzed using the same approach as was used for the decomposition to vinyl and methyl radicals. The potential energy profiles of the reaction path of the H-atom elimination reaction are shown in Figure 5S. The length of the breaking C-H bond was used as a reaction coordinate for this process. The QCISD(T) energies obtained were scaled with the experimental-to-calculated ratio of the energy of the products of this reaction and fitted with expression II. The result of the fitting is presented as a solid line in the lower plot of Figure

5S. The coefficients of the polynomial expression II and calculated and experimental energy values are provided in Table 5S.

Rotational Constants

The rotational constants of the structures located on the reaction paths of the propene decomposition reactions were calculated using the B3PW91-level IRC geometries. Each structure was presented as a symmetric top described by one 1-dimensional (1D) and one 2-dimensional (2D) rotational degrees of freedom. The rotational constants of the 2D rotations were calculated as the geometric mean of the two (similar in value) rotational constants corresponding to the principal moments of inertia. The rotational constants of the internal 1D rotor (relative rotation of the methyl and vinyl fragments about the axis of the breaking C-C bond) were calculated using the formulas of Pitzer and Gwinn.[24]

The dependence of each rotational constant on the reaction coordinate was interpolated with a polynomial function:

$$B = \sum_{i=0}^{4} b_i R^i \qquad \text{(III)}$$

where R is the corresponding reaction coordinate and b_i are the fitting coefficients. The obtained coefficients of the polynomial expression III are provided in Table 5S.

Vibrational Frequencies

Projected[22,23] B3PW91/6-31G(d,p)-level vibrational frequencies were calculated for the structures located on the IRC reaction paths of the barrierless propene decomposition channels (reactions –A and D in scheme II of the article). The vibrational modes of each structure were matched with those of the preceding and the following structure on the reaction path to ensure adequate description of the evolution of projected frequencies along the reaction coordinate. The results of these frequency calculations are presented in Figures 6S and 7S. For each reaction channel, the vibrational modes were subdivided into two categories: transitional and non-transitional. The transitional modes correspond to the relative "rocking" motion of the separating fragments and evolve into rotational degrees of freedom at the products end of the reaction path. Their frequencies approach zero as the distance between the fragments increases. There are four transitional modes (numbers 1, 2, 3, and 4 in Table 5S) in the reaction path of decomposition of propene to C_2H_3 and CH_3 and two in that of decomposition to H and C_3H_5 (numbers 1 and 2 in Table 5S). One more transitional mode, that of the one-dimensional relative torsional rotation of

the $-C_2H_3$ and $-CH_3$ fragments, has very low frequencies (5 – 90 cm^{-1} within the considered 3.8 – 2.3 Å range of the reaction coordinate) and, therefore, was approximated by a free internal rotor for the purpose of calculation of the microcanonical rate constants.

The non-transitional modes converge to the normal modes of the products as the distance between the departing fragments increases. Some of the non-transitional modes showed virtually no dependence on the reaction coordinate (within the considered range) and were essentially equal to the corresponding frequencies of the products. These modes (not shown in Figures 6S and 7S) were considered as conserved.

The dependence of the frequency of each non-conserved vibrational mode on the reaction coordinate was fitted with the same type of polynomial function as was used for the interpolation of the rotational constants (expression V). The results of the frequency interpolations are shown as solid lines in Figures 6S and 7S. A correspondence was established between the non-transitional vibrational modes and the corresponding normal modes of the products to which they converge at infinite separation of the fragments. The coefficients of the polynomial representation of each non-transitional mode were scaled with the ratio of the experimental to calculated frequencies of the corresponding vibrational mode of the products. The scaled coefficients, together with the corresponding experimental and calculated frequencies of the products, and the unscaled coefficients of the polynomial representation of the transitional modes are provided in Table 5S. Mode assignment of the experimental frequencies of the allyl radical necessary for matching of the experimental and calculated frequencies was taken from reference 25.

The scaling procedure was performed in order to reduce errors in the calculated frequencies and to ensure that the calculated potential energy along the reaction paths, with ZPE included, converges to the experimental energy of the products in the limit of infinite separation of the fragments. For the same reason, the conserved non-transitional vibrational modes were assigned the experimental frequencies of the corresponding modes of the products (Table 5S). The experimental frequencies of the products were used in the scaling procedure rather than the experimental frequencies of the reactant because it was anticipated that the transition states selected by the variational approach will be closer to products (in terms of structure).

IIS.3. Microcanonical Rate Constants

Details of calculations and relevant formulas

The RRKM method applied to such a reaction model results in the following expression for the microcanonical rate constants:

$$k(E,J) = \frac{W^{\neq}(E + E_{rot})}{h\rho(E)} \equiv \frac{\int_0^{E+E_{rot}} \rho^{\neq}(E')dE'}{h\rho(E)} \qquad \text{(IV)}$$

where

$$E_{rot} = (B\text{-}B^{\neq})J(J+1) \qquad \text{(V)}$$

is the difference between the energy of adiabatic two-dimensional rotation of the propene molecule and that of the transition state. Here, J is the quantum number of the total angular momentum (J is conserved during the course of reaction.); $W^{\neq}(E)$ is the sum of states of the active degrees of freedom of the transition state at energy E; $\rho(E)$ and $\rho^{\neq}(E)$ are the densities of states of active degrees of freedom of the reacting molecule and transition state, respectively; B and $B^{\neq}$ are the rotational constants of the adiabatic rotations in the same species; and h is the Planck constant.

The $k_{-A}(E,J)$ values were averaged over the Boltzmann rotational distribution of propene using the formula

$$k_{-A}(E,T) = \sum_{J=0}^{\infty} k_{-A}(E,J)(2J+1)\exp\left(-\frac{BJ(J+1)}{k_B T}\right) \qquad \text{(VI)}$$

where B is the rotational constant of the two-dimensional adiabatic rotation. A finite rather than the infinite sum in expression VI was used in numerical computation. The upper limit of summation (maximum J number) was chosen in such a way that an increase of this number by 30 % would produce less than a 1% change in the high-pressure-limit rate constant of the unimolecular channel calculated by the numerical integration of the $k_{-A}(E,T)$ function over the Boltzmann distribution of active degrees of freedom of the propene molecule.

Harmonic treatment of the rocking transitional modes

At large separations of the fragments, the vibrational frequencies of the transitional

modes of both decomposition channels are low in value (Figures 6S and 7S) indicating possibly large anharmonicities of these degrees of freedom. Accurate treatment of such degrees of freedom would require a rather detailed knowledge of their potential energy surfaces, knowledge which is currently unavailable. The treatment of these "rocking" types of motion with the simple harmonic oscillator models used in this work is associated with potential errors that are not easily estimated. Several considerations, however, indicate that these errors of harmonic treatment can be expected not to be dramatic. First, these transitional anharmonic degrees of freedom affect only calculation of the sum-of-states functions of the transition states, $W^{\neq}(E)$. The important energy range of the $W^{\neq}(E)$ function is significantly narrower than that of the $\rho(E)$ function because it extends from the reaction barrier (or critical energy below which $W^{\neq}(E)$ is zero) and up to the approximate "end" of the energy distribution of the chemically activated propene molecules formed in the C_2H_3 + CH_3 recombination. Second, the $W^{\neq}(E)$ functions are mostly affected by the low-energy part of the density-of-states functions of the individual degrees of freedom, where harmonic approximation is most adequate. This can be seen from the convolution formula for the sum-of-states function $W_{1,2}(E)=\int_0^E W_1(E-\varepsilon)\rho_2(\varepsilon)d\varepsilon$ (see, for example, ref. [13]). Here, $\rho_2(\varepsilon)$ and $W_1(\varepsilon)$ are the density of states of the anharmonic degree of freedom under consideration and the sum of states of all other degrees of freedom in the molecule. Since $W_1(\varepsilon)$ grows with energy at a much faster rate than the $\rho_2(\varepsilon)$ (due to accounting for many degrees of freedom), the main contributions to the integral are provided by the low ε part of the $0 - E$ integration interval, where $W_1(E-\varepsilon)$ is large. Finally, application of a variational approach to the calculation of the energy-dependent rate constants partially compensates for the anharmonic behavior of these degrees of freedom: as the energy increases, the position of the transition state shifts toward the reactant (propene) side, where the frequencies of the transitional modes are higher and the harmonic model gives better representation.

IIS.3. Contribution of Isomerization at T > 900 K.

In order to estimate the contribution of the isomerization channel under the conditions where the virtual component formalism had to be applied (T > 900 K), the channel branching ratios were also calculated using the first computational approach (with the reversible

isomerization included, see text of the article). The calculations were performed after the parameters of the reaction model (including the parameters of the collisional energy transfer) were adjusted to reproduce the experimental data on the $C_2H_3 + CH_3$ combination reaction. The results obtained at the pressures of 1, 1000, and 10000 Torr in the 900 – 3000 K temperature range indicate that the time-dependent rate of formation of cyclopropane decreases with time as the system approaches thermal equilibrium and never exceeds 10 % of the rate of formation of stabilized propene. The calculated branching fractions of other reaction channels also change with time, as expected, but the time-dependent rate values obtained after a short induction period ($<10^{-5}$ s) are not sensitive to whether the reversible isomerization is included in the computational scheme. Thus, the isomerization channel can be excluded from the kinetic scheme of the $C_2H_3 + CH_3$ combination reaction for the purpose of the application of the virtual component formalism without serious implications for the accuracy of the computed results. The main effect of this exclusion is that the calculated rates of stabilized propene formation account for the formation of both propene and cyclopropene without distinguishing between these two isomers.

References

1. Curtiss, L. A.; Raghavachari, K.; Trucks, G. W.; Pople, J. A. *J. Chem. Phys.* **1991**, *94*, 7221.
2. Pople, J. A.; Gead-Gordon, M.; Raghavachari, K. *J. Chem. Phys.* **1987**, *87*, 5968.
3. Perdew, J. P.; Wang, Y. *Phys. Rev. B* **1992**, *34*, 13244.
4. Becke, A. D. *J. Chem. Phys.* **1992**, *97*, 9173.
5. Cui, Q.; Liu, Z.; Morokuma, K. *J. Chem. Phys.* **1998**, *109*, 56.
6. Durant, J. L. *Computational Thermochemistry: Prediction and Estimation of Molecular Thermodynamics*ACS Symposium Series: Washington, DC, 1998.
7. Fukui, K. *Acc. Chem. Res.* **1981**, *14*, 363.
8. Gonzalez, C.; Schlegel, H. B. *J. Phys. Chem.* **1990**, *94*, 5523.
9. Frisch, M. J.; Trucks, G. W.; Schlegel, H. B.; Scuseria, G. E.; Robb, M. A.; Cheeseman, J. R.; Zakrzewski, V. G.; Montgomery, J. A. Jr.; Stratmann, R. E.; Burant, J. C.; Dapprich, S.; Millam, J. M.; Daniels, A. D.; Kudin, K. N.; Strain, M. C.; Farkas, O.; Tomasi, J.; Barone, V.; Cossi, M.; Cammi, R.; Mennucci, B.; Pomelli, C.; Adamo, C.; Clifford, S.; Ochterski, J.; Petersson, G. A.; Ayala, P. Y.; Cui, Q.; Morokuma, K.; Malick, D. K.; Rabuck, A. D.; Raghavachari, K.; Foresman, J. B.; Cioslowski, J.; Ortiz, J. V.; Stefanov, B. B.; Liu, G.; Liashenko, A.; Piskorz, P.; Komaromi, I.; Gomperts, R.; Martin, R. L.; Fox, D. J.; Keith, T.; Al-Laham, M. A.; Peng, C. Y.; Nanayakkara, A.; Gonzalez, C.; Challacombe, M.; Gill, P. M. W.; Johnson, B.; Chen, W.; Wong, M. W.; Andres, J. L.; Head-Gordon, M.; Replogle, E. S.; Pople, J. A. *Gaussian 98, Revision A.3;* Gaussian, Inc.: Pittsburgh, PA, 1998.
10. Frisch, M. J.; Trucks, G. W.; Schlegel, H. B.; Gill, P. M. W.; Johnson, B. G.; Robb, M. A.; Cheeseman, J. R.; Keith, T.; Petersson, G. A.; Montgomery, J. A.; Raghavachari, K.; Al-Laham, M. A.; Zakrzewski, V. G.; Ortiz, J. V.; Foresman, J. B.; Cioslowski, J.; Stefanov, B. B.; Nanayakkara, A.; Challacombe, M.; Peng, C. Y.; Ayala, P. Y.; Chen, W.; Wong, M. W.;

Andres, J. L.; Replogle, E. S.; Gomperts, R.; Martin, R. L.; Fox, D. J.; Binkley, J. S.; Defrees, D. J.; Baker, J.; Stewart, J. P.; Head-Gordon, M.; Gonzalez, C.; Pople, J. A. *Gaussian 94, Revision E.1;* Gaussian, Inc.: Pittsburgh, PA, 1995.

11. Dubnikova, F.; Lifshitz, A. *J. Phys. Chem.* **1998**, *102*, 3299.
12. Furue, H.; Pacey, P. D. *Can. J. Chem.* **1982**, *60*, 916.
13. Gilbert, R. G.; Smith, S. C. *Theory of Unimolecular and Recombination Reactions;* Blackwell: Oxford, 1990.
14. Robinson, P. J.; Holbrook, K. A. *Unimolecular Reactions;* Wiley-interscience: New York, 1972.
15. Stoliarov, S. I.; Knyazev, V. D.; Slagle, I. R. *J. Phys. Chem.* **2000**, *104*, 9687.
16. Fahr, A.; Laufer, A. H.; Klein, R.; Braun, W. *J. Phys. Chem.* **1991**, *95*, 3218.
17. Fahr, A.; Braun, W.; Laufer, A. H. *J. Phys. Chem.* **1993**, *97*, 1502.
18. Thorn, R. P. Jt.; Payne, W. A. Jr.; Chillier, X. D. F.; Stief, L. J.; Nesbitt, F. L.; Tardy, D. C. *Int. J. Chem. Kinet.* **2000**, *32*, 304.
19. Fahr, A.; Laufer, A. H.; Tardy, D. C. *J. Phys. Chem.* **1999**, *103*, 8433.
20. Wang, H. *Private Communication* **1999**.
21. Peterson, G. A. *Computational Thermochemistry: Prediction and Estimation of Molecular Thermodynamics*ACS Symposium Series: Washington, DC, 1998.
22. Miller, H. W.; Handy, N. C.; Adams, J. E. *J. Chem. Phys.* **1980**, *72*, 99.
23. Baboul, A. G.; Schlegel, H. B. *J. Chem. Phys.* **1997**, *107*, 9413.
24. Pitzer, K. S.; Gwinn, W. D. *J. Chem. Phys.* **1942**, *10*, 428.
25. Liu, X.; Getty, J. D.; Kelly, P. B. *J. Chem. Phys.* **1993**, *99*, 1522.
26. Chao, J.; Zwolinski, B. J. *J. Phys. Chem. Ref. Data* **1975**, *4*, 251.
27. Brupbacher, T.; Styger, C.; Vogelsanger, B.; Ozier, I.; Bauder, A. *J. Mol. Spectrosc.* **1989**, *138*, 197.
28. Ervin, K. M.; Gronert, S.; Barlow, S. E.; Gilles, M. K.; Harrison, A. G.; Bierbaum, V. M.; DePuy, C. H.; Lineberger, W. C.; Ellison, G. B. *J. Am. Chem. Soc.* **1990**, *112*, 5750.
29. Chase, M. W. Jr.; Davies, C. A.; Downey, J. R. Jr.; Frurip, D. J.; McDonald, R. A.; Syverud, A. N. *JANAF Thermochemical Tables, 3rd Ed.; J. Phys. Chem. Ref. Data* **1985**, *14*, (Suppl. No. 1).
30. Shimanouchi, T. *Tables of Molecular Vibrational Frequencies. Consolidated Volume I;* National Bureau of Standards: Gaithersburg, 1972.
31. Uy, D.; Davis, S.; Nesbitt, D. J. *J. Chem. Phys.* **1998**, *109*, 7793.
32. Reid, R. C.; Prausnitz, J. M.; Sherwood, T. K. *The Properties of Gases and Liquids, 3rd Ed.*; McGraw-Hill: New York, 1977.
33. Rabinovitch, B. S.; Diesen, R. W. *J. Chem. Phys.* **1959**, *30*, 735.

Table 1S. Optimized Geometries of Transition States and Intermediates Involved in the C_2H_3+CH_3 Reaction.

TS 1

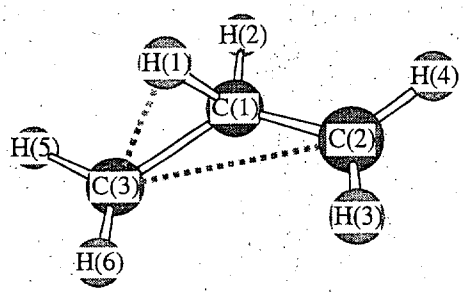

Structure	Parameters[a]	MP2/6-31G(d)	B3PW91/6-31G(d,p)
TS 1	c2c1	1.4087	1.4183
	c3c1	1.4799	1.4774
	c3c1c2	126.3221	127.8984
	h1c1	1.1959	1.1739
	h1c1c3	67.2856	73.7786
	h1c1c3c2	-101.0235	-100.9227
	h2c1	1.0885	1.0921
	h2c1c2	116.8786	115.4795
	h2c1c2c3	-160.5455	-159.2101
	h3c2	1.0833	1.0851
	h3c2c1	121.3055	121.4924
	h3c2c1c3	-13.1707	-13.9349
	h4c2	1.0807	1.0827
	h4c2c1	120.2524	119.847
	h4c2c1c3	-183.5056	-184.5869
	h5c3	1.0799	1.0831
	h5c3c1	119.2224	118.6408
	h5c3c1c2	181.7941	179.195
	h6c3	1.0816	1.0849
	h6c3c1	119.6625	120.0126
	h6c3c1c2	17.7919	18.3917

[a] Here and throughout this table: Parameters are: x#y# - distance between atoms X# and Y# (Å); x#y#z# - angle between bonds X#Y# and Y#Z# (deg); x#y#z#w# - dihedral angle determined by atoms X#, Y#, Z#, W# (deg).

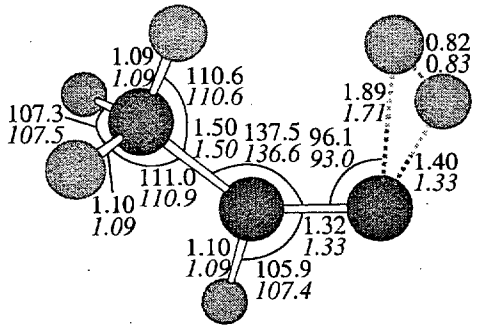

TS 2.1

Structure	Parameters	MP2/6-31G(d)	B3PW91/6-31G(d,p)
TS 2.1	c2c1	1.4975	1.496
	h3c2	1.0938	1.0937
	h3c2c1	110.6389	110.6216
	h4c2	1.0943	1.0958
	h4c2c1	110.9035	110.9927
	h4c2c1h3	-120.3194	-120.3961
	h5c2	1.0943	1.0958
	h5c2c1	110.9035	110.9927
	h5c2c1h3	120.3194	120.3961
	h6c1	1.0944	1.0994
	h6c1c2	115.9752	116.6276
	h6c1c2h3	180.0	180.0
	c7c1	1.3329	1.3187
	c7c1h6	107.4166	105.8767
	c7c1h6c2	180.0	180.0
	h8c1	1.714	1.8942
	h8c7c1	93.0111	96.1049
	h8c7c1h6	180.0	180.0
	h9c7	1.3271	1.4015
	h9c7h8	28.0957	23.1193
	h9c7h8c1	180.0	180.0

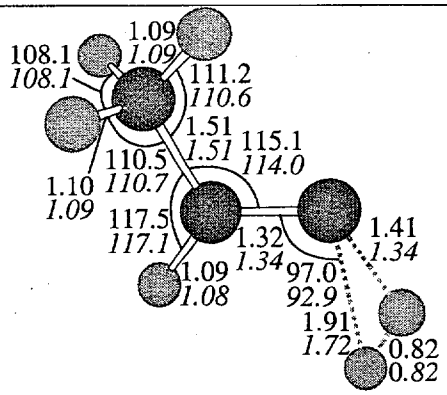

TS 2.2

Structure	Parameters	MP2/6-31G(d)	B3PW91/6-31G(d,p)
TS 2.2	c2c1	1.5072	1.5108
	h3c2	1.0932	1.0937
	h3c2c1	110.6191	111.2338
	h4c2	1.0938	1.0954
	h4c2c1	110.6829	110.5052
	h4c2c1h3	-120.0958	-120.196
	h5c2	1.0938	1.0954
	h5c2c1	110.6829	110.5052
	h5c2c1h3	120.0958	120.196
	h6c1	1.084	1.085
	h6c1c2	117.1256	117.4547

TS 2.2	h6c1c2h3	180.0	180.0
	c7c1	1.3377	1.3239
	c7c1h6	128.9129	127.481
	c7c1h6c2	180.0	180.0
	h8c1	1.7212	1.912
	h8c7c1	92.9397	96.9813
	h8c7c1h6	0.0	0.0
	h9c7	1.3424	1.4088
	h9c7h8	27.6464	22.5074
	h9c7h8c1	180.0	180.0

TS 2.3

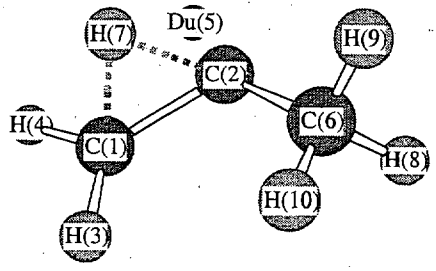

Structure	Parameters	MP2/6-31G(d)	B3PW91/6-31G(d,p)
TS 2.3	c2c1	1.3951	1.3972
	h3c1	1.1024	1.1063
	h3c1c2	124.4972	124.8819
	h4c1	1.0905	1.0932
	h4c1c2	120.26	119.9824
	h4c1c2h3	187.6354	188.9019
	[du]5c2[b]	1.0	1.0
	[du]5c2c1[b]	90.0	90.0
	[du]5c2c1h4[b]	0.0	0.0
	c6c2	1.5032	1.4989
	c6c2[du]5[b]	156.9665	155.6904
	c6c2[du]5c1[b]	170.8114	171.0229
	h7c2	1.3208	1.3398
	h7c2c6	113.0336	113.9361
	h7c2c6c1	60.1391	60.1351
	h8c6	1.0961	1.0987
	h8c6c2	105.2675	105.1874
	h8c6c2h7	172.1096	174.2061
	h9c6	1.0928	1.095
	h9c6c2	111.7734	111.767
	h9c6c2h8	114.5301	113.4481
	h10c6	1.1028	1.1053
	h10c6c2	116.2925	117.1534
	h10c6c2h8	-119.0108	-119.217

CH_3CCH_3

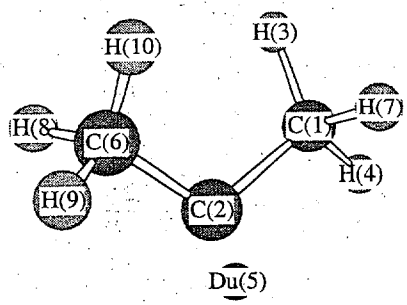

Structure	Parameters	MP2/6-31G(d)	B3PW91/6-31G(d,p)
CH_3CCH_3	c2c1	1.484	1.4797
	h3c1	1.1	1.1036
	h3c1c2	113.7489	115.5543
	h4c1	1.0918	1.095
	h4c1c2	113.0579	113.2315
	h4c1c2h3	234.2213	232.1075
	[du]5c2[b]	1.0	1.0
	[du]5c2c1[b]	90.0	90.0
	[du]5c2c1h4[b]	0.0	0.0
	c6c2	1.484	1.4797
	c6c2[du]5[b]	149.3509	145.2316
	c6c2[du]5c1[b]	144.775	139.6306
	h7c2	2.0816	2.0679
	h7c2c6	106.8788	111.2248
	h7c2c6c1	31.6479	33.5243
	h8c6	1.1012	1.1045
	h8c6c2	106.3147	105.4013
	h8c6c2h7	113.1583	121.8569
	h9c6	1.0919	1.095
	h9c6c2	113.0573	113.2535
	h9c6c2h8	117.3922	115.5647
	h10c6	1.1	1.1036
	h10c6c2	113.754	115.5115
	h10c6c2h8	-116.8266	-116.5813

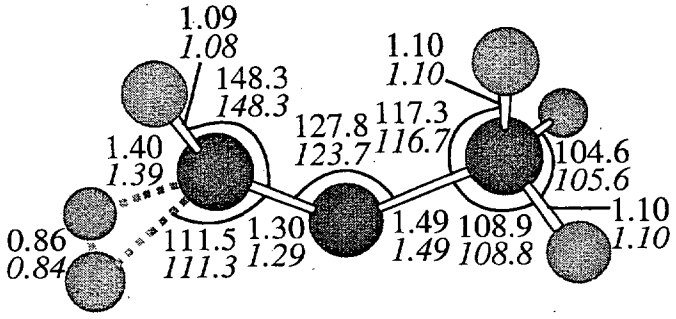

TS 2.4

Structure	Parameters	MP2/6-31G(d)	B3PW91/6-31G(d,p)
TS 2.4	c2c1	1.2924	1.2952
	h3c1	1.3897	1.3948
	h3c1c2	111.324	111.4883
	h4c1	1.3897	1.3948
	h4c1c2	111.3242	111.4872
	h4c1c2h3	322.3589	321.4857
	c6c2	1.4938	1.4846
	c6c2x5	141.9587	138.2347
	c6c2x5c1	205.8227	203.0361
	h7c2	2.2871	2.2901
	h7c2c6	109.2548	113.3776
	h7c2c6c1	0.0	0.0
	h8c6	1.0946	1.0972
	h8c6c2	108.7847	108.8742
	h8c6c2h7	122.7204	123.2624
	h9c6	1.0946	1.0972
	h9c6c2	108.785	108.8723
	h9c6c2h8	114.5562	113.4876
	h10c6	1.099	1.1013
	h10c6c2	116.6542	117.3319
	h10c6c2h8	-122.7217	-123.2572

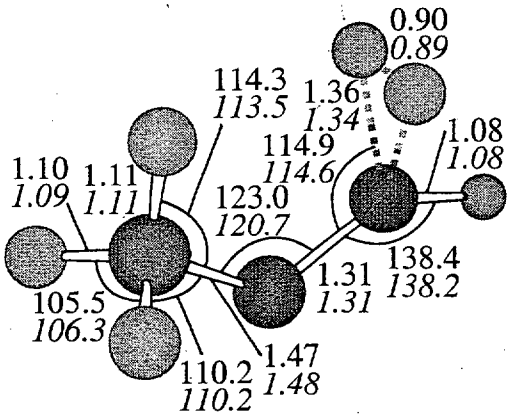

TS 2.5

Structure	Parameters	MP2/6-31G(d)	B3PW91/6-31G(d,p)
TS 2.5	c2c1	1.3081	1.3109
	h3c1	1.338	1.3556
	h3c1c2	114.5936	114.8735
	h4c1	1.338	1.3556
	h4c1c2	114.5935	114.8731
	h4c1c2h3	316.9451	317.1446
	c6c2	1.4795	1.4743
	c6c2x5	31.3204	33.5286
	c6c2x5c1	169.1612	170.2105

TS 2.5	h7c2	2.2313	2.2366
	h7c2c6	139.4802	141.6534
	h7c2c6c1	0.0001	-0.0001
	h8c6	1.0941	1.0965
	h8c6c2	110.181	110.1653
	h8c6c2h7	121.5294	122.036
	h9c6	1.0941	1.0965
	h9c6c2	110.1809	110.165
	h9c6c2h8	116.9421	115.9305
	h10c6	1.1127	1.113
	h10c6c2	113.517	114.3368
	h10c6c2h8	-121.529	-122.035

TS 3.1

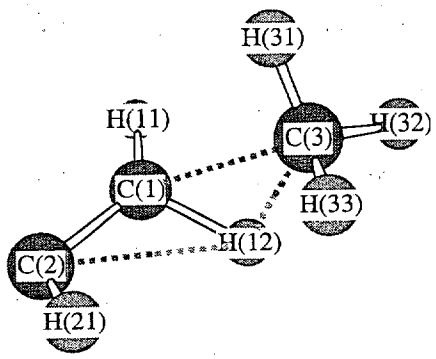

Structure	Parameters	MP2/6-31G(d)	B3PW91/6-31G(d,p)
TS 3.1	c2c1	1.3338	1.3376
	c3c1	1.8878	1.9144
	c3c1c2	123.2581	124.6701
	h11c1	1.083	1.0853
	h11c1c2	130.5726	130.0974
	h11c1c2c3	-157.4807	-159.5072
	h12c1	1.178	1.1669
	h12c1c2	113.9928	112.1045
	h12c1c2c3	53.8888	54.9023
	h21c2	1.0988	1.1003
	h21c2c1	114.0401	114.7701
	h21c2c1c3	-17.8532	-16.2955
	h31c3	1.0858	1.0865
	h31c3c1	93.9884	94.3076
	h31c3c1c2	-98.0207	-95.0753
	h32c3	1.0937	1.0929
	h32c3c1	118.5123	116.0077
	h32c3c1c2	-213.8623	-210.7769
	h33c3	1.0902	1.0905
	h33c3c1	108.4436	110.135
	h33c3c1c2	16.1085	19.4855

TS 3.2

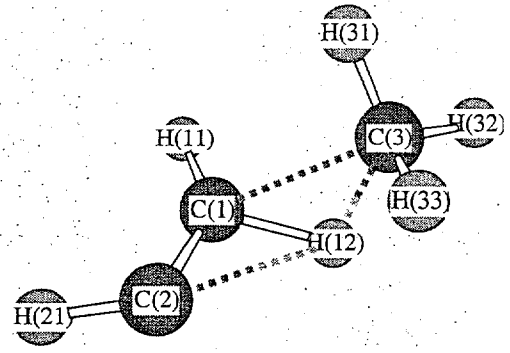

Structure	Parameters	MP2/6-31G(d)	B3PW91/6-31G(d,p)
TS 3.2	c2c1	1.3293	1.3316
	c3c1	1.8741	1.8872
	c3c1c2	111.4564	112.394
	h11c1	1.0879	1.09
	h11c1c2	142.0515	141.6519
	h11c1c2c3	-156.2626	-156.5567
	h12c1	1.2042	1.1997
	h12c1c2	108.9161	108.3673
	h12c1c2c3	46.3472	47.7109
	h21c2	1.1	1.1022
	h21c2c1	109.8644	110.4904
	h21c2c1c3	163.4702	164.3217
	h31c3	1.0842	1.0854
	h31c3c1	93.624	93.9561
	h31c3c1c2	-107.8373	-103.632
	h32c3	1.0963	1.0962
	h32c3c1	122.4272	120.4357
	h32c3c1c2	-224.0268	-219.4391
	h33c3	1.0878	1.0888
	h33c3c1	103.4674	105.3987
	h33c3c1c2	6.0165	10.085

TS 3.3

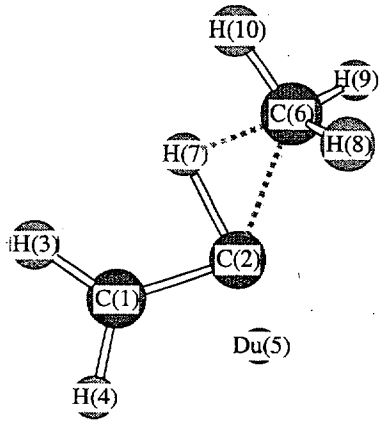

Structure	Parameters	MP2/6-31G(d)	B3PW91/6-31G(d,p)
TS 3.3	c2c1	1.3707	1.3581
	h3c1	1.0986	1.0984
	h3c1c2	128.2486	129.8885
	h4c1	1.0896	1.0918
	h4c1c2	118.0142	116.6499
	h4c1c2h3	177.1826	177.3844
	[du]5c2[b]	1.0	1.0
	[du]5c2c1[b]	90.0	90.0
	[du]5c2c1h4[b]	0.0	0.0
	c6c2	1.6874	1.6949
	c6c2[du]5[b]	152.4041	146.6956
	c6c2[du]5c1[b]	161.4657	167.6027
	h7c2	1.2102	1.2313
	h7c2c6	52.1647	49.8327
	h7c2c6c1	49.5052	36.5817
	h8c6	1.0888	1.0896
	h8c6c2	97.6706	98.1496
	h8c6c2h7	151.9332	139.7945
	h9c6	1.0875	1.0874
	h9c6c2	108.5774	106.0031
	h9c6c2h8	113.8348	114.0335
	h10c6	1.11	1.1164
	h10c6c2	124.0695	127.3712
	h10c6c2h8	-115.7089	-116.8899

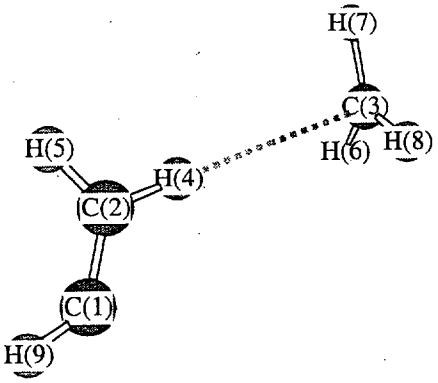

INT 4.1, MP2 structure

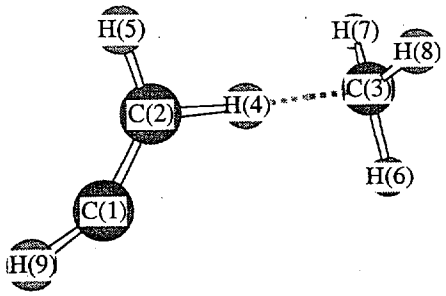

TS 4.1, MP2 structure

Parameters	INT 4.1, MP2/6-31G(d) structure	TS 4.1, MP2/6-31G(d) structure
c2c1	1.2871	1.2575
c3c2	3.9333	2.7539
c3c2c1	121.5074	121.4303
h4c2	1.0868	1.2107
h4c2c1	122.3587	119.8236
h4c2c1c3	0.0003	0.0
h5c2	1.0912	1.0885

h5c2h4	116.001	109.2906
h5c2h4c1	180.0	180.0
h6c3	1.0787	1.0843
h6c3c2	87.2796	100.6198
h6c3c2c1	60.0795	0.0
h7c3	1.0787	1.0841
h7c3c2	99.947	102.5562
h7c3c2h6	119.9314	119.7281
h8c3	1.0787	1.0841
h8c3c2	87.2764	102.5562
h8c3c2h6	-120.1377	-119.7281
h9c1	1.0804	1.0731
h9c1h5	110.3637	128.8183
h9c1h5c2	180.0	180.0

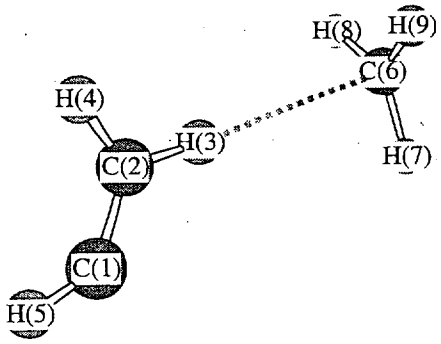

INT 4.1, B3PW91 structure

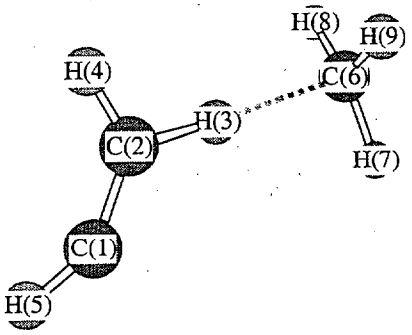

TS 4.1, B3PW91 structure

Parameters	INT 4.1, B3PW91/6-31G(d,p) structure	TS 4.1, B3PW91/6-31G(d,p) structure
c2c1	1.309	1.289
h3c2	1.0927	1.1569
h3c2c1	122.2384	121.2083
h4c2	1.0949	1.093
h4c2h3	115.8122	112.0268
h4c2h3c1	179.9996	180.0094
h5c1	1.0827	1.0775
h5c1h4	111.6559	122.2437
h5c1h4c2	180.0008	179.996
c6h3	2.7174	1.7631
c6h3h4	145.3405	143.2431
c6h3h4h5	180.141	180.0559
h7c6	1.0823	1.0847
h7c6h3	88.2678	96.5256
h7c6h3c1	-6.5438	-3.7148
h8c6	1.0823	1.0847
h8c6h3	92.799	99.577
h8c6h3c1	113.3346	115.9503

h9c6	1.0823	1.0847
h9c6h3	93.3195	99.7204
h9c6h3c1	-126.4176	-123.4106

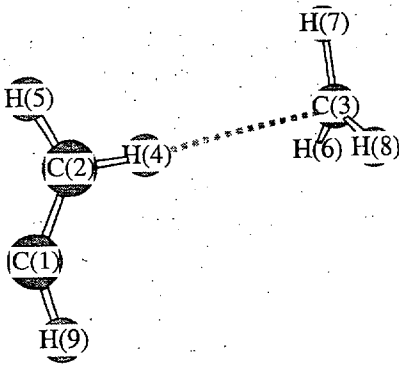

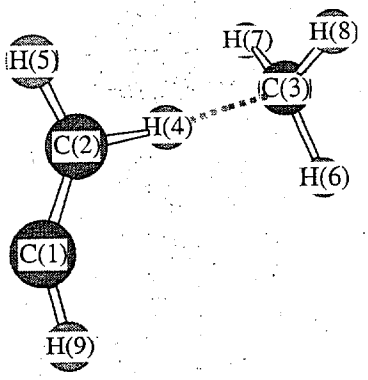

	INT 4.2, MP2 structure	**TS 4.2**, MP2 structure
Parameters	INT 4.2, MP2/6-31G(d) structure	TS 4.2, MP2/6-31G(d) structure
c2c1	1.2871	1.267
c3c2	3.865	2.7807
c3c2c1	124.6524	125.0065
h4c2	1.092	1.1962
h4c2c1	122.0056	121.3479
h4c2c1c3	0.0112	0.0
h5c2	1.0865	1.0849
h5c2h4	115.9888	111.0537
h5c2h4c1	180.0	180.0
h6c3	1.0788	1.0838
h6c3c2	91.5951	102.2999
h6c3c2c1	60.0489	0.0
h7c3	1.0788	1.0835
h7c3c2	92.4642	101.037
h7c3c2h6	119.9989	120.095
h8c3	1.0788	1.0835
h8c3c2	91.5433	101.037
h8c3c2h6	-120.004	-120.095
h9c1	1.0804	1.0773
h9c1h4	110.3822	112.7786
h9c1h4c2	179.9999	180.0

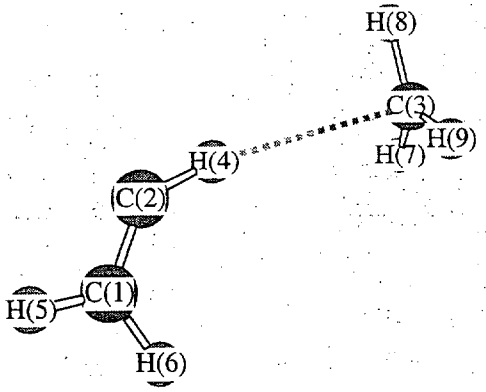

INT 4.3, MP2 structure

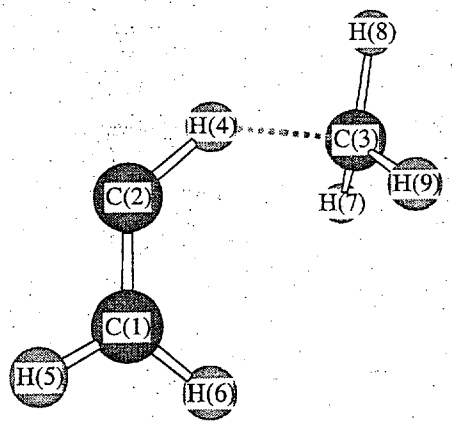

TS 4.3, MP2 structure

Parameters[a]	INT 4.3, MP2/6-31G(d) structure	TS 4.3, MP2/6-31G(d) structure
c2c1	1.2872	1.2884
c3c2	3.8157	2.5416
c3c2c1	129.0414	105.7335
h4c2	1.0815	1.1717
h4c2c1	137.0978	129.5596
h4c2c1c3	-0.0009	0.0006
h5c1	1.0864	1.0867
h5c1c2	122.2286	119.7721
h5c1c2c3	180.0009	179.9983
h6c1	1.091	1.0884
h6c1c2	121.8514	124.0869
h6c1c2c3	0.0009	-0.0014
h7c3	1.0788	1.0831
h7c3c2	90.7569	95.452
h7c3c2c1	59.9331	58.3807
h8c3	1.0789	1.085
h8c3c2	95.1682	114.5367
h8c3c2h6	179.9911	179.9171
h9c3	1.0788	1.0831
h9c3c2	90.7601	95.4825
h9c3c2h6	-59.951	-58.5263

[a] Here and throughout this table: Parameters are: x#y# - distance between atoms X# and Y# (Å); x#y#z# - angle between bonds X#Y# and Y#Z# (deg); x#y#z#w# - dihedral angle determined by atoms X#, Y#, Z#, W# (deg).

[b] [du]# (Du#) - dummy atom.

Table 2S. Calculated Vibrational Frequencies (cm^{-1}) of Reactants, Products, Transition States and Intermediates of the C_2H_3+CH_3 Reaction

Species	HF/6-31G(d) Frequencies[a]	B3PW91/6-31G(d,p) Frequencies
C_2H_3	828, 885, 959, 1196, 1408, 1635, 3279, 3374, 3431	722, 826, 921, 1060, 1398, 1675, 3084, 3182, 3268
CH_3	305, 1540, 1540, 3286, 3463, 3463	467, 1414, 1414, 3139, 3326, 3326
CH_3CHCH_2	210, 455, 641, 986, 1029, 1068, 1129, 1187, 1297, 1443, 1555, 1594, 1625, 1639, 1881, 3195, 3242, 3274, 3319, 3333, 3404	208, 423, 588, 937, 938, 945, 1033, 1068, 1194, 1329, 1410, 1455, 1487, 1501, 1741, 3038, 3099, 3134, 3152, 3162, 3247
CH_2CHCH_2	451, 547, 572, 780, 799, 1005, 1035, 1075, 1251, 1342, 1537, 1638, 1648, 3325, 3326, 3337, 3419, 3423	425, 531, 551, 777, 802, 934, 1010, 1044, 1220, 1278, 1424, 1527, 1530, 3160, 3167, 3173, 3270, 3272
c-C_3H_6[b]	804, 804, 922, 962, 962, 1191, 1191, 1224, 1268, 1304, 1330, 1330, 1616, 1616, 1680, 3309, 3309, 3323, 3383, 3383, 3405	739, 739, 861, 912, 912, 1062, 1064, 1083, 1154, 1214, 1214, 1238, 1478, 1479, 1534, 3152, 3152, 3160, 3233, 3233, 3253
CH_3CCH	393, 393, 795, 795, 985, 1167, 1167, 1565, 1625, 1625, 2419, 3216, 3285, 3285, 3666	349, 349, 621, 621, 960, 1053, 1053, 1417, 1483, 1483, 2251, 3049, 3124, 3124, 3499
H_2	4646	4456
C_2H_2	794, 794, 882, 882, 2247, 3607, 3720	584, 584, 772, 772, 2087, 3443, 3544
CH_4	1487, 1487, 1487, 1702, 1702, 3200, 3305, 3305, 3305	1347, 1347, 1347, 1574, 1574, 3054, 3183, 3183, 3183
CH_2C	635, 941, 1398, 1843, 3326, 3410	315, 751, 1220, 1723, 3153, 3236
CH_3CCH_3	80, 173, 365, 911, 937, 969, 1016, 1243, 1288, 1531, 1539, 1599, 1615, 1618, 1635, 3148, 3157, 3194, 3201, 3271, 3272	127, 135, 341, 727, 798, 918, 970, 1112, 1219, 1358, 1360, 1434, 1435, 1489, 1492, 2965, 2970, 3029, 3031, 3110, 3112
TS 1	2177*i*,[c] 391, 439, 515, 554, 629, 942, 982, 987, 1268, 1311, 1364, 1525, 1589, 1646, 2060, 3327, 3338, 3351, 3423, 3469	1494*i*,[c] 349, 397, 531, 572, 599, 821, 917, 942, 1181, 1247, 1274, 1413, 1475, 1528, 2453, 3138, 3181, 3183, 3287, 3298
TS 2.1	1194*i*,[c] 149, 484, 545, 585, 781, 982, 1005, 1176, 1200, 1407, 1564, 1620, 1633, 1742, 2040, 3122, 3197, 3254, 3266, 3305	476*i*,[c] 152, 356, 425, 584, 601, 774, 929, 991, 1054, 1191, 1284, 1409, 1480, 1493, 1771, 3045, 3081, 3117, 3143, 3233
TS 2.2	1150*i*,[c] 231, 449, 467, 535, 765, 1001, 1022, 1181, 1201, 1421, 1559, 1626, 1626, 1748, 1983, 3193, 3199, 3248, 3291, 3350	476*i*,[c] 249, 318, 359, 546, 580, 814, 953, 1030, 1051, 1188, 1304, 1406, 1488, 1489, 1688, 3048, 3122, 3143, 3218, 3274

Species	HF/6-31G(d) Frequencies[a]	B3PW91/6-31G(d,p) Frequencies
TS 2.3	1448*i*,[c] 149, 456, 673, 982, 1120, 1144, 1173, 1284, 1457, 1538, 1555, 1624, 1637, 1693, 2347, 3135, 3196, 3232, 3265, 3338	1054*i*,[c] 176, 421, 604, 920, 1006, 1028, 1068, 1171, 1330, 1389, 1416, 1467, 1497, 1531, 2269, 2954, 2957, 3078, 3118, 3138
TS 2.4	1505*i*,[c] 109, 308, 446, 604, 855, 972, 1046, 1127, 1175, 1469, 1529, 1542, 1630, 1637, 1745, 3163, 3236, 3260, 3463, 3565	1458*i*,[c] 35, 314, 392, 618, 830, 878, 986, 1047, 1085, 1315, 1385, 1394, 1490, 1491, 1767, 2989, 3011, 3076, 3100, 3204
TS 2.5	1680*i*,[c] 211, 388, 526, 601, 956, 1010, 1093, 1121, 1189, 1475, 1534, 1551, 1622, 1625, 1740, 3075, 3134, 3235, 3267, 3514	1468*i*,[c] 222, 325, 387, 596, 878, 897, 973, 1007, 1086, 1259, 1349, 1396, 1467, 1481, 1698, 2713, 2874, 3077, 3113, 3307
TS 3.1	1443*i*,[c] 113, 338, 596, 683, 857, 1041, 1113, 1194, 1301, 1408, 1462, 1596, 1636, 1665, 2473, 3229, 3240, 3353, 3409, 3433	1275*i*,[c] 120, 293, 501, 571, 803, 930, 967, 1001, 1130, 1227, 1337, 1449, 1480, 1549, 2553, 3069, 3074, 3199, 3218, 3234
TS 3.2	1109*i*,[c] 134, 361, 608, 730, 872, 1009, 1091, 1238, 1305, 1409, 1449, 1599, 1628, 1768, 2447, 3203, 3230, 3367, 3390, 3430	1071*i*,[c] 146, 330, 542, 658, 802, 949, 982, 1056, 1144, 1264, 1306, 1444, 1493, 1616, 2406, 3055, 3058, 3141, 3196, 3248
TS 3.3	1154*i*,[c] 121, 274, 461, 780, 1066, 1121, 1162, 1206, 1271, 1501, 1580, 1618, 1634, 1735, 2539, 3140, 3224, 3300, 3330, 3362	675*i*,[c] 153, 254, 499, 806, 875, 948, 1031, 1090, 1255, 1358, 1467, 1475, 1553, 1615, 2308, 2845, 3033, 3135, 3146, 3217
TS 3.4	1086*i*,[c] 638, 1024, 1995, 2758, 3599	907*i*,[c] 595, 924, 1869, 2575, 3386
TS 4.1	2436*i*,[c] 30, 184, 345, 462, 587, 631, 720, 736, 1080, 1250, 1259, 1465, 1549, 1575, 1586, 3243, 3350, 3378, 3378, 3484	462*i*,[c] 26, 154, 249, 449, 476, 501, 748, 761, 963, 1010, 1352, 1421, 1421, 1647, 1976, 3114, 3120, 3296, 3296, 3334

Species	HF/6-31G(d) Frequencies[a]	B3PW91/6-31G(d,p) Frequencies
INT 4.1	5, 22, 43, 44, 76, 95, 358, 830, 885, 966, 1198, 1408, 1540, 1541, 1635, 3276, 3284, 3373, 3428, 3460, 3461	7, 43, 57, 80, 131, 153, 509, 720, 821, 937, 1057, 1400, 1414, 1414, 1674, 3067, 3138, 3139, 3268, 3325, 3326
TS 4.2	2303*i*,[c] 21, 179, 349, 461, 595, 651, 860, 874, 1124, 1211, 1231, 1458, 1557, 1572, 1584, 3246, 3382, 3385, 3389, 3466	
INT 4.2	7, 24, 42, 48, 78, 105, 370, 831, 888, 963, 1198, 1408, 1541, 1541, 1635, 3277, 3284, 3371, 3428, 3460, 3460	
TS 4.3	2604*i*,[c] 20, 172, 356, 521, 643, 650, 978, 994, 1259, 1279, 1420, 1528, 1578, 1581, 1679, 3249, 3310, 3383, 3385, 3388	
INT 4.3	8, 22, 43, 48, 83, 98, 383, 833, 893, 960, 1197, 1408, 1541, 1541, 1635, 3277, 3284, 3371, 3430, 3460, 3460	

[a] Unscaled HF/6-31G(d) frequencies. [b] Cyclopropane. [c] Imaginary frequency.

Table 3S. Energies (Hartree) of Reactants, Products, Intermediates, and Transition States of the C_2H_3+CH_3 Reaction Calculated by the G2 and the QCISD(T)//B3PW91 Methods

Species	G2		QCISD(T)//B3PW91		$\langle S^2 \rangle$ [e]
	G2 Energy [a]	HF ZPE [b]	QCISD(T) Energy [c]	B3PW91 ZPE [d]	
C_2H_3	-77.774395	0.034572	-77.746085	0.036761	0.93
			-77.745259[f]		
CH_3	-39.772737	0.027657	-39.755779	0.029812	0.76
			-39.755807[f]		
CH_3CHCH_2	-117.721385	0.076303	-117.670355	0.079939	0.00
CH_2CHCH_2	-117.067953	0.062063	-117.022251	0.066280	0.96
H	-0.500000		-0.499810		0.75
c-C_3H_6[g]	-117.709068	0.077938	-117.657231	0.081708	0.00
CH_3CCH	-116.472823	0.053665	-116.427191	0.055671	0.00
H_2	-1.175898	0.009540	-1.170822	0.010152	0.00
C_2H_2	-77.212025	0.026293	-77.183411	0.026849	0.00
CH_4	-40.453549	0.042682	-40.431316	0.045086	0.00
CH_2C	-77.140792	0.023500	-77.112245	0.023688	0.18
CH_3CCH_3	-117.608834	0.072741	-117.556389	0.075476	0.69
TS 1	-117.601532	0.067351	-117.538002	0.072409	0.86
TS 2.1	-117.562271	0.067245	-117.510098	0.068605	0.00
TS 2.2	-117.560977	0.067316	-117.508413	0.068958	0.00
TS 2.3	-117.599193	0.071194	-117.547078	0.074128	0.00
TS 2.4	-117.532603	0.066882	-117.480422	0.069268	0.00
TS 2.5	-117.548057	0.066858	-117.496130	0.068582	0.00
TS 3.1	-117.534624	0.069447	-117.482702	0.072229	0.00
TS 3.2	-117.532713	0.069707	-117.480884	0.072528	0.00
TS 3.3	-117.543566	0.070026	-117.491532	0.073044	0.00
TS 3.4	-77.136959	0.020370	-77.107195	0.021300	0.00

[a] Energy calculated at the G2 [1] level of theory (MP2/6-31G(d)-level optimized structure). Zero-point vibrational energy is not included. 1 hartree = 2625.5 kJ mol^{-1}.

[b] Zero-point vibrational energy calculated at the HF/6-31G(d) level of theory and scaled with a factor of 0.8929. The computed frequencies are presented in Table 2S.

[c] Energy calculated at the QCISD(T)/6-311+G(2df,2p) level of theory for B3PW91/6-31G(d,p) optimized structure. Zero-point vibrational energy is not included.

[d] Zero-point vibrational energy calculated at the B3PW91/6-31G(d,p) level of theory. The computed frequencies are presented in Table 2S.

[e] $\langle S^2 \rangle = S(S+1)$ value at the UHF/6-31G(d) level of theory before the annihilation of the first spin contaminant (for MP2/6-31G(d) optimized structure).

[f] Energy calculated at the QCISD(T)/6-311+G(2df,2p) level of theory for MP2/6-31G(d) optimized structure.

[g] Cyclopropane.

Table 4S. Calculated Energies of Transition States and Intermediates Involved in the Abstraction of H-atom from C_2H_3 by CH_3

Species	G2		QCISD(T)		$\langle S^2 \rangle$[e]	G2 ΔE[f]		QCISD(T) ΔE[f]	
	G2 Energy[a]	HF ZPE[b]	QCISD(T) Energy[c]	B3PW91 ZPE[d]		ZPE not included	ZPE included	ZPE not included	ZPE is included[g]
TS 4.1	-117.552781	0.061619	-117.495091	0.066779	1.10	-14.83	-16.43	17.78	18.32
INT 4.1	-117.563763	0.062913	-117.502888	0.067618	1.20	-43.66	-41.87	-2.69	0.06
TS 4.2	-117.559220	0.062237	-117.499258		1.11	-31.74	-31.72	4.75	4.77
INT 4.2	-117.563265	0.062979	-117.502316		1.19	-42.36	-40.39	-3.28	-1.31
TS 4.3	-117.561650	0.063825	-117.501275		0.94	-38.12	-33.93	-0.55	3.64
INT 4.3	-117.559886	0.063008	-117.502339		1.19	-33.49	-31.44	-3.34	-1.30

[a] G2 energy in Hartree. Zero-point vibrational energy is not included. In the cases of transition states the calculations were performed for the structures at the top of QCISD(T)/6-311G(d,p)//MP2/6-31G(d) IRC barriers (See text for details.). [b] HF/6-31G(d) zero-point vibrational energy in Hartree scaled by a factor 0.8929.

[c] QCISD(T)/6-311+G(2df,2p)//B3PW91/6-31G(d,p) energy in Hartree. Zero-point vibrational energy is not included. If the structure could not be located on the B3PW91 potential energy surface, the same geometry as in the G2 calculation was used (see text for details), in which case energy relative to reactants was obtained by subtracting the QCISD(T)/6-311+G(2df,2p)//MP2/6-31G(d) energy of $C_2H_3 + CH_3$. [d] B3PW91/6-31G(d,p) zero-point vibrational energy in Hartree. [e] $\langle S^2 \rangle = S(S+1)$ value at UHF/6-31G(d) level of theory before the annihilation of the first spin contaminant (for MP2/6-31G(d) optimized structure). [f] Relative energy in kJ mol^{-1} with respect to the C_2H_3+CH_3 reactants. [g] HF ZPE is used if B3PW91 ZPE is not available.

Table 5S. Parameters of the Model of the $C_2H_3 + CH_3 \rightarrow$ *Products* Reaction and the Reaction of Propene Decomposition.

Reaction Critical Energies, kJ mol^{-1} (Experimental [a] / Calculated [b])

$E_D(C_3H_6 \rightarrow C_2H_3+CH_3)$ = 445.6 / 436.7 $E_{-A}(C_3H_6 \rightarrow H+C_3H_5)$ = 399.2 / 387.1 $E_I(C_3H_6 \rightarrow$ cyclo-$C_3H_6)$ = 336.3 [c]

Polynomial Representation (Formula II) of the Potential Energy Profiles Along the Reaction Paths (Units are kJ mol^{-1} and Å)

$C_3H_6 \rightarrow C_2H_3+CH_3$:	a_1 =	-3.0306×10^3	a_2 =	6.5671×10^4	a_3 =	-6.0643×10^5	a_4 =	3.0922×10^6
	a_5 =	-9.3977×10^6	a_6 =	1.7013×10^7	a_7 =	-1.6978×10^7	a_8 =	7.2013×10^6
$C_3H_6 \rightarrow H+C_3H_5$:	a_1 =	-5.6710×10^2	a_2 =	1.0025×10^4	a_3 =	-7.5449×10^4	a_4 =	3.1312×10^5
	a_5 =	-7.7304×10^5	a_6 =	1.1340×10^6	a_7 =	-9.1384×10^5	a_8 =	3.1183×10^5

Rotational Constants [d] (cm^{-1}) or their Polynomial Representations [e] (Formula III, units are cm^{-1} and Å), Symmetry Numbers (given in parentheses if not unity), and Torsional Barrier (V_0, in kJ mol^{-1})

C_3H_6:[26]	(2D)	0.2902	(1D)	1.544	(1D Internal) 7.096 (3) V_0 = 8.355
C_3H_5:[25]	(2D)	0.3157 (2)	(1D)	1.829	
cyclo-C_3H_6:[27]	(2D)	0.6734 (3)	(1D)	0.4211 (2)	
C_2H_3:[28]	(2D)	0.9976	(1D)	7.4909	
CH_3: [29]	(2D)	9.5771 (2)	(1D)	4.788 (3)	

$C_3H_6 \rightarrow$ cyclo-C_3H_6 Transition State: (2D) 0.2827 (1D) 1.592

$C_3H_6 \rightarrow H+C_3H_5$ Transition State: (2D) $b_0 = 0.2874$, $b_1 = 0.004679$, $b_2 = -0.0005931$, $b_3 = -0.002006$, $b_4 = 0.0003276$

(1D) $b_0 = 1.756$, $b_1 = -0.02919$, $b_2 = -0.1430$, $b_3 = 0.02824$, $b_4 = -0.001469$

$C_3H_6 \rightarrow C_2H_3+CH_3$ Transition State: (2D) $b_0 = 0.5748$, $b_1 = -0.3411$, $b_2 = 0.1084$, $b_3 = -0.01955$, $b_4 = 0.001513$

(1D) $b_0 = 2.355$, $b_1 = 0.3091$, $b_2 = -0.7117$, $b_3 = 0.2560$, $b_4 = -0.02856$

(1D Internal) $b_0 = 9.811$, $b_1 = 0.1885$, $b_2 = -1.547$, $b_3 = 0.5733$, $b_4 = -0.06278$

Vibrational Frequencies (cm^{-1}) and Degeneracies (in parentheses)

C_3H_6:[26]	3091, 3022, 2991, 2973, 2953, 2932, 1653, 1459, 1443, 1414, 1378, 1298, 1178, 1045, 990, 935, 919, 912, 575, 428, 188 (torsion)
cyclo-C_3H_6:[30]	3103, 3082(2), 3038, 3025(2), 1479, 1438(2), 1188(3), 1126, 1070, 1029(2), 866(2), 854, 739(2)
C_3H_5:[31]	3107(2), 3054, 3021, 3019, 1487, 1464, 1390, 1247, 1182, 1071, 983, 912, 801, 738, 544, 514, 426
C_2H_3:[28]	3265, 3190, 3115, 1670, 1445, 1185, 920, 825, 785
CH_3:[29]	3184(2), 3002, 1383(2), 580
$C_3H_6 \rightarrow$ cyclo-C_3H_6 Transition State:	527[349], 550[397], 560[531], 580[572], 599, 821, 917, 942, 1181, 1247, 1274, 1413, 1475, 1528, 2453, 3138, 3181, 3183, 3287, 3298

Table 5S (continued). Parameters of the Model of the $C_2H_3 + CH_3 \rightarrow$ *Products* Reaction and the Reaction of Propene Decomposition.

Coefficients of the Polynomial Representations of Vibrational Frequencies[f] (Formula V, units are cm^{-1} and Å)

$C_3H_6 \rightarrow C_2H_3 + CH_3$ Reaction:

Vibrational mode	Coefficients of Polynomial	Experimental / Calculated Frequency of Product, cm^{-1}
1[g]	$b_0 = -247.2$, $b_1 = 1190.0$, $b_2 = -804.3$, $b_3 = 198.9$, $b_4 = -17.0$	
	[$b_0 = -514.9$, $b_1 = 2479.1$, $b_2 = -1675.6$, $b_3 = 414.3$, $b_4 = -35.5$]	
2[g]	$b_0 = -3025.4$, $b_1 = 5279.8$, $b_2 = -2931.7$, $b_3 = 674.8$, $b_4 = -56.1$	
	[$b_0 = -6303.0$, $b_1 = 10999.5$, $b_2 = -6107.8$, $b_3 = 1405.9$, $b_4 = -116.9$]	
3[g]	$b_0 = -3538.9$, $b_1 = 6627.4$, $b_2 = -3754.3$, $b_3 = 866.9$, $b_4 = -71.8$	
	[$b_0 = -7222.2$, $b_1 = 13525.3$, $b_2 = -7661.8$, $b_3 = 1769.2$, $b_4 = -146.5$]	
4[g]	$b_0 = -3549.4$, $b_1 = 6965.5$, $b_2 = -4041.1$, $b_3 = 949.1$, $b_4 = -79.6$	
	[$b_0 = -7170.5$, $b_1 = 14071.8$, $b_2 = -8163.8$, $b_3 = 1917.4$, $b_4 = -160.9$]	
5[h]	$b_0 = -16208.0$, $b_1 = 27325.1$, $b_2 = -14804.8$, $b_3 = 3346.4$, $b_4 = -272.8$	580 / 467 (CH_3)
6[h]	$b_0 = 4317.6$, $b_1 = -1989.1$, $b_2 = 49.8$, $b_3 = 132.1$, $b_4 = -18.9$	785 / 722 (C_2H_3)
7[h]	$b_0 = -841.4$, $b_1 = 2716.0$, $b_2 = -1477.4$, $b_3 = 336.5$, $b_4 = -27.7$	825 / 826 (C_2H_3)
8[h]	$b_0 = 5942.6$, $b_1 = -5653.2$, $b_2 = 2390.0$, $b_3 = -449.6$, $b_4 = 31.7$	920 / 921 (C_2H_3)
9[h]	$b_0 = 17439.9$, $b_1 = -19470.9$, $b_2 = 8785.7$, $b_3 = -1766.4$, $b_4 = 133.3$	1185 / 1060 (C_2H_3)
10	Conserved	1445 / 1398 (C_2H_3)
11[h]	$b_0 = 2482.2$, $b_1 = -981.6$, $b_2 = 310.5$, $b_3 = -39.4$, $b_4 = 1.5$	1383 / 1413 (CH_3)
12[h]	$b_0 = 2427.5$, $b_1 = -907.6$, $b_2 = 272.2$, $b_3 = -30.4$, $b_4 = 0.7$	1383 / 1414 (CH_3)
13[h]	$b_0 = 2287.2$, $b_1 = -1681.8$, $b_2 = 1118.3$, $b_3 = -285.6$, $b_4 = 25.4$	1670 / 1675 (C_2H_3)
14	conserved	3115 / 3085 (C_2H_3)
15	conserved	3002 / 3140 (CH_3)
16	conserved	3190 / 3183 (C_2H_3)
17[h]	$b_0 = 701.6$, $b_1 = 2550.3$, $b_2 = -952.6$, $b_3 = 159.4$, $b_4 = -10.2$	3265 / 3269 (C_2H_3)
18	conserved	3184 / 3327 (CH_3)
19	conserved	3184 / 3327 (CH_3)

Table 5S (continued). Parameters of the Model of the $C_2H_3 + CH_3 \rightarrow$ *Products* Reaction and the Reaction of Propene Decomposition.

$C_3H_6 \rightarrow H + C_3H_5$ Reaction:

Vibrational mode	Coefficients of Polynomial	Experimental / Calculated Frequency of Product, cm^{-1}
1 [g]	$b_0 = -4055.2$, $b_1 = 6997.2$, $b_2 = -4063.4$, $b_3 = 997.6$, $b_4 = -89.4$	
	[$b_0 = -7798.5$, $b_1 = 13456.1$, $b_2 = -7814.3$, $b_3 = 1918.5$, $b_4 = -171.9$]	
2 [g]	$b_0 = -13863.4$, $b_1 = 23367.0$, $b_2 = -13990.2$, $b_3 = 3615.9$, $b_4 = -344.2$	
	[$b_0 = -24493.6$, $b_1 = 41289.7$, $b_2 = -24717.6$, $b_3 = 6388.5$, $b_4 = -608.2$]	
3 [h]	$b_0 = -122.6$, $b_1 = 645.4$, $b_2 = -276.8$, $b_3 = 50.4$, $b_4 = -3.2$	426 / 425
4 [h]	$b_0 = 24300.4$, $b_1 = -34218.8$, $b_2 = 18538.4$, $b_3 = -4472.1$, $b_4 = 404.7$	514 / 531
5 [h]	$b_0 = 31216.4$, $b_1 = -42650.1$, $b_2 = 22363.6$, $b_3 = -5232.5$, $b_4 = 460.3$	544 / 551
6 [h]	$b_0 = -8822.7$, $b_1 = 17114.8$, $b_2 = -10937.0$, $b_3 = 3004.1$, $b_4 = -301.9$	738 / 777
7 [h]	$b_0 = 11234.3$, $b_1 = -14707.4$, $b_2 = 7875.2$, $b_3 = -1889.4$, $b_4 = 170.8$	801 / 802
8	conserved	912 / 934
9	conserved	983 / 1010
10 [h]	$b_0 = 12727.4$, $b_1 = -18027.5$, $b_2 = 10368.7$, $b_3 = -2630.9$, $b_4 = 248.6$	1071 / 1044
11 [h]	$b_0 = 2621.3$, $b_1 = -2029.7$, $b_2 = 1092.8$, $b_3 = -264.8$, $b_4 = 24.3$	1182 / 1220
12h [c]	$b_0 = 1713.3$, $b_1 = -260.3$, $b_2 = -57.6$, $b_3 = 56.2$, $b_4 = -8.4$	1247 / 1278
13	conserved	1390 / 1423
14	conserved	1464 / 1527
15 [h]	$b_0 = 12617.7$, $b_1 = -16330.5$, $b_2 = 9022.3$, $b_3 = -2219.2$, $b_4 = 204.7$	1487 / 1530
16	conserved	3054 / 3162
17	conserved	3019 / 3167
18	conserved	3021 / 3174
19	conserved	3107 / 3271
20	conserved	3107 / 3273

Table 5S (continued). Parameters of the Model of the $C_2H_3 + CH_3 \rightarrow$ *Products* Reaction and the Reaction of Propene Decomposition.

Lennard-Jones Parameters [32]

Gas	ε/k, K	σ, Å
He	10.22	2.551
Kr	178.9	3.655
Propene	298.9	4.678
Cyclopropane	248.9	4.807

[a] $\Delta E = \Delta_f H^0$ (products) - ZPE(products) - ($\Delta_f H^0$ (propene) - ZPE(propene)) calculated using experimental $\Delta_f H^0$ at T = 0 K and experimental frequencies of corresponding species.

[b] Relative energy of products with respect to propene calculated at the QCISD(T)/6-311G(d,p)//B3PW91/6-31G(d,p) level of theory. ZPE is not included.

[c] Isomerization barrier obtained from fitting of the high-pressure-limit expression of Furue and Pacey.[12]

[d] All species are presented as symmetric tops described by one 2-dimensional (2D) and one 1-dimensional (1D) external rotational constant.

[e] For the barrierless processes, coefficients of polynomial expression V describing the dependence of rotational constants (cm^{-1}) on the reaction coordinate (Å) are provided.

[f] Coefficients of polynomial expression V describing the dependence of vibrational frequencies (cm^{-1}) on the reaction coordinate (Å) for the barrierless propene decomposition channels.

[g] Coefficients of polynomial are adjusted to reproduce the high-pressure-limit rate constant (see text). Unadjusted coefficients are given in square brackets.

[h] Coefficients of polynomial are scaled with the corresponding ratio of experimental frequency to calculated frequency of product.

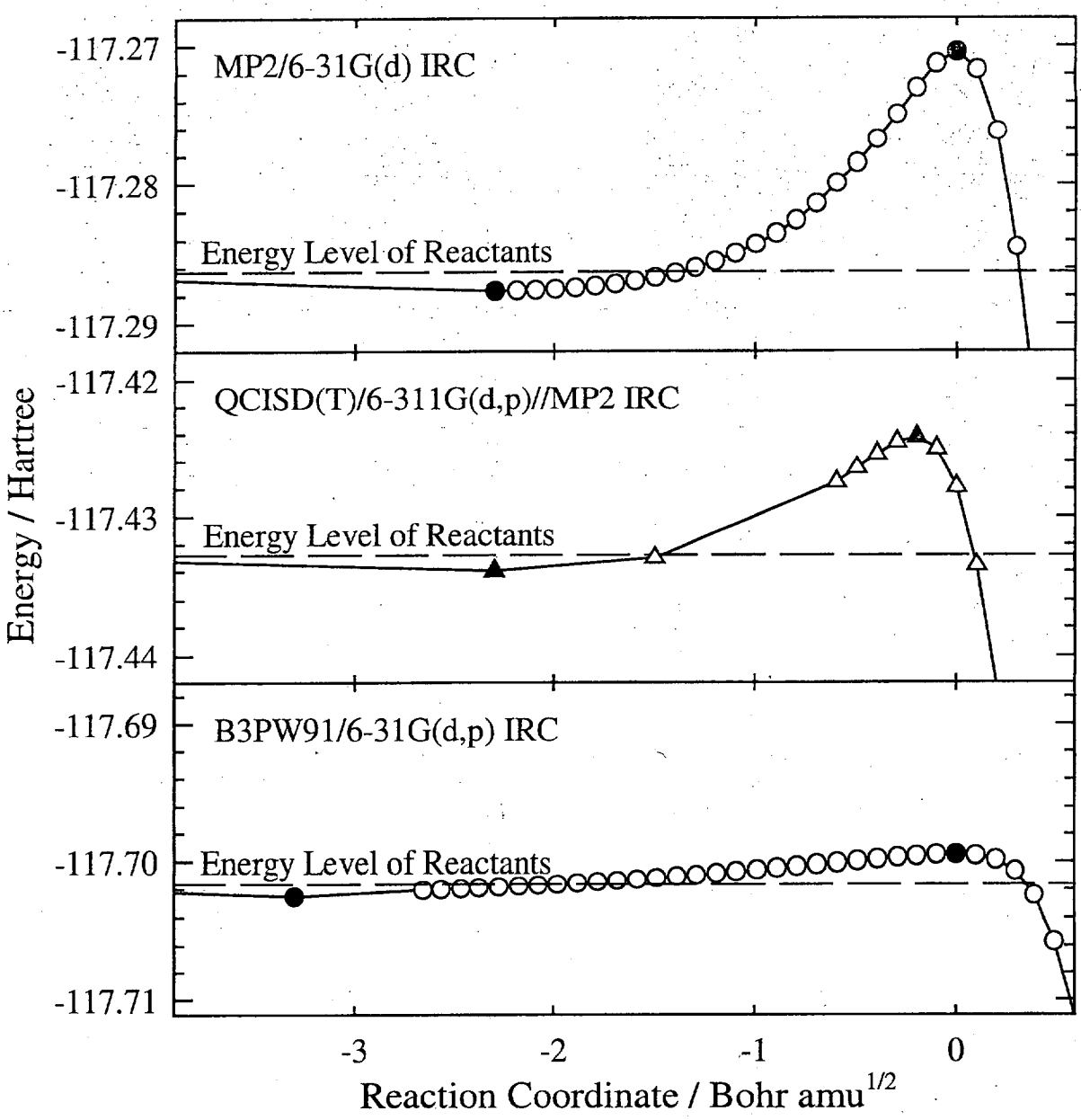

Figure 1S. Potential energy profiles of the first channel (abstraction of the H atom in the trans position from the $=CH_2$ group) of the $C_2H_3 + CH_3 \rightarrow C_2H_2 + CH_4$ reaction. Filled circles and triangles signify the positions of minima and maxima of potential energy. 1 hartree = 2625.5 kJ mol^{-1}.